Hindawi Publishing Corporation
Journal of Sensors
Volume 2016, Article ID 7964727, 11 pages
http://dx.doi.org/10.1155/2016/7964727

Research Article

A Model Reference Adaptive Control/PID Compound Scheme on Disturbance Rejection for an Aerial Inertially Stabilized Platform

Xiangyang Zhou, Chao Yang, and Tongtong Cai

School of Instrumentation Science & Opto-Electronics Engineering, Beihang University, Beijing 100191, China

Correspondence should be addressed to Xiangyang Zhou; xyzhou@buaa.edu.cn

Received 17 June 2016; Revised 14 August 2016; Accepted 4 September 2016

Academic Editor: Rafael Morales

This paper describes a method to suppress the effect of nonlinear and time-varying mass unbalance torque disturbance on the dynamic performances of an aerial inertially stabilized platform (ISP). To improve the tracking accuracy and robustness of the ISP, a compound control scheme based on both of model reference adaptive control (MRAC) and PID control methods is proposed. The dynamic model is first developed which reveals the unbalance torque disturbance with the characteristic of being nonlinear and time-varying. Then, the MRAC/PID compound controller is designed, in which the PID parameters are adaptively adjusted based on the output errors between the reference model and the actual system. In this way, the position errors derived from the prominent unbalance torque disturbance are corrected in real time so that the tracking accuracy is improved. To verify the method, the simulations and experiments are, respectively, carried out. The results show that the compound scheme has good ability in mass unbalance disturbance rejection, by which the system obtains higher stability accuracy compared with the PID method.

1. Introduction

For an aerial remote sensing system, due to the serious effects of internal and external disturbances, the movement of the aircraft is not ideal that makes the sensor's line of sight (LOS) jitter, eventually resulting in the degradation of images quality [1–4]. In order to obtain high-resolution images and satisfy the requirements of high photo overlapping ratio, the sensor's LOS must be strictly controlled. Therefore, inertially stabilized platform (ISP) is a key component for the high-precision aerial remote sense imaging system, which is used to hold and control the LOS of the imaging sensor to keep steady relative to the inertial space or the tracked target [5, 6]. The ISP with high control precision is indispensable for isolating disturbances derived from diverse sources [7, 8], particularly for the case of swings of three angular attitudes of aircraft. It is a principal issue for the control system of ISP of how to minimize the effects of disturbances introduced on the ISP [2].

The most critical performance metric for an ISP is torque disturbance rejection. It is difficult for the conventional PID control method in low speed servo motion to suppress these complex nonlinear disturbances. It is hard for the traditional feedforward control method to further improve the ISP's dynamic performance [9]. Therefore, there is continuous interest for researchers to develop the control methods with higher accuracy and stability by various disturbances rejection. The development of computer technology and advanced intelligent control theory provide a new way for the control of complex dynamic uncertain systems and the disturbance rejection. They have been gradually used in the control of ISP, such as neural network [10], genetic algorithm [11, 12], fuzzy control [13, 14], robust control [15], state compensation control [16], and autodisturbance rejection control [17]. Predictive control and fuzzy control are the effective methods to optimize the control of uncertain systems. The combination of the two methods can enable the system to have the quicker dynamic response and smaller overshot [11–14]. For a system characterized by nonlinear and time-varying behavior, the issue of stability performance becomes very prominent. In [1], the decoupling compensation controller obtains a good result in which the angular velocity

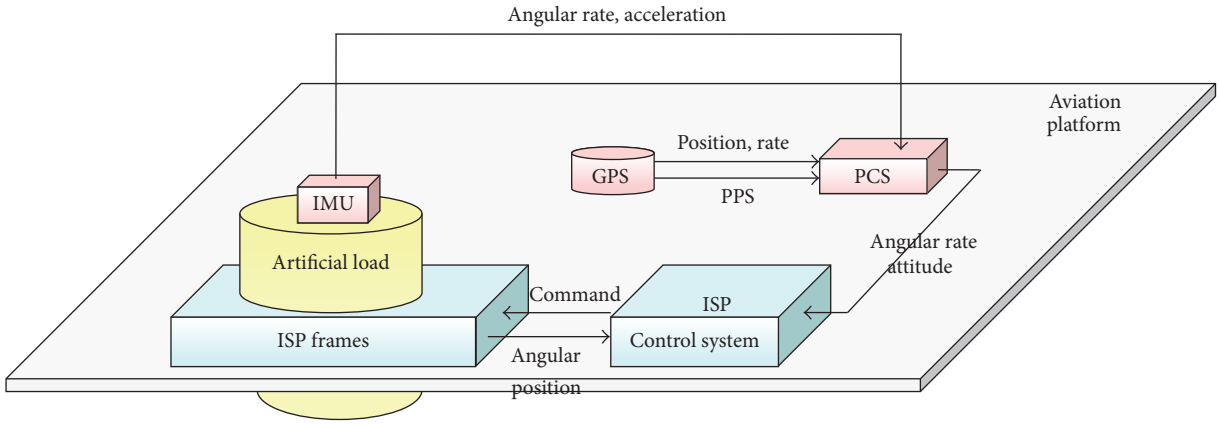

Figure 1: Schematic diagram of an aerial remote sensing system.

coupling, torque coupling, and moment of inertia coupling are considered. In [18], a three-closed loop PID compound control scheme is applied to a two-axis ISP to obtain the desired results. In [19], a feedforward compensation scheme is proposed to achieve vibration rejection of ISP. In [20], an active disturbance rejection control strategy is put forward to improve robustness of electrode regulator system.

Disturbances arise from diverse sources; for example, the angular motion and linear vibration of aircraft platform generate the disturbance torques due to mass unbalance and gimbal geometry [4, 5]. Generally, the influence of unbalance torque is prominent over other disturbances. Since the centroid is not exactly coincident with the center of the rotating axis, the mass unbalance torque will occur when ISP operates, which will severely degrade the system control accuracy. To compensate the mass unbalance torque, the static equilibrium test is required before the operation. However, due to many nonideal cases such as different imaging sensors being installed interchangeably, it is hard to completely eliminate the unbalance torque by static equilibrium mass correction. Moreover, since the mass unbalance torque is a nonlinear and time-varying disturbance, it is difficult for the conventional control to solve it [21]. Therefore, it is necessary to compensate the mass unbalance torque by using the intelligent control methods which have strong adaptive disturbance rejection ability. Previously, some methods have been proposed to compensate the unbalance torques, such as the adaptive control based on disturbance observer [22], the neural network control [10], the feedforward control [23], independent mechanisms [24], fuzzy inference mechanism [25], iterative feedback tuning of fuzzy control [26], adaptive neural network control [27], and so on.

Model reference adaptive control (MRAC) can restrain the influences of external disturbance by effectively revising the model parameter errors. MRAC does not need the online identification of the mathematical model of mass unbalance torque, by which the time of adaptive control is greatly shortened. Therefore, MRAC is appropriate for the occasion of parameters change [21]. In MRAC, an adaptive reference model needs to be designed which can achieve the desired performance index with the same order of the plant. In [28], a MRAC system based on the certainty equivalent (CE) principle for the first-order delay system is proposed. MRAC/PID compound control scheme is a combination of adaptive control and traditional PID control, which can make the PID parameters of the nonlinear time-varying uncertain systems adjusted in real time, so as to improve the system robustness and control accuracy. MRAC/PID controller owns the great robust ability for the nonlinear, hysteresis, and variable parameters systems. Compared with the conventional PID control method, the MRAC/PID controller can tune the PID parameters automatically and make the system stable in the whole working range [29].

In this paper, to improve the tracking accuracy and robustness of an aerial inertially stabilized platform, a MRAC/PID compound control scheme is proposed to weaken the influence of prominent unbalance torque disturbance. The dynamic model is first developed which reveals the unbalance torque disturbance with the characteristic of being nonlinear and time-varying. Then, a MRAC/PID compound controller is designed and simulation analysis is conducted. To verify the method, the experiments are carried out.

2. Background

2.1. Aerial Remote Sensing System. Figure 1 shows the schematic diagram of an aerial remote sensing system. Generally, an aerial remote sensing system consists of four main components, a three-axis ISP, an imaging sensor, a position and orientation system (POS), and the aviation platform. When applied, the three-axis ISP is mounted on the aviation platform, and the imaging sensor and POS are mounted on inner azimuth gimbal of the ISP. When the aviation platform rotates or jitters, the control system of three-axis ISP gets the high-precision attitude reference information measured by POS and then routinely controls the LOS of imaging sensor to achieve accurate pointing and stabilizing relative to ground level and flight track. The POS, which is mainly composed of three main components, that is, inertial measurement unit (IMU), GPS receiving antenna, and data processing system, is used to provide an accurate reference of position and attitude

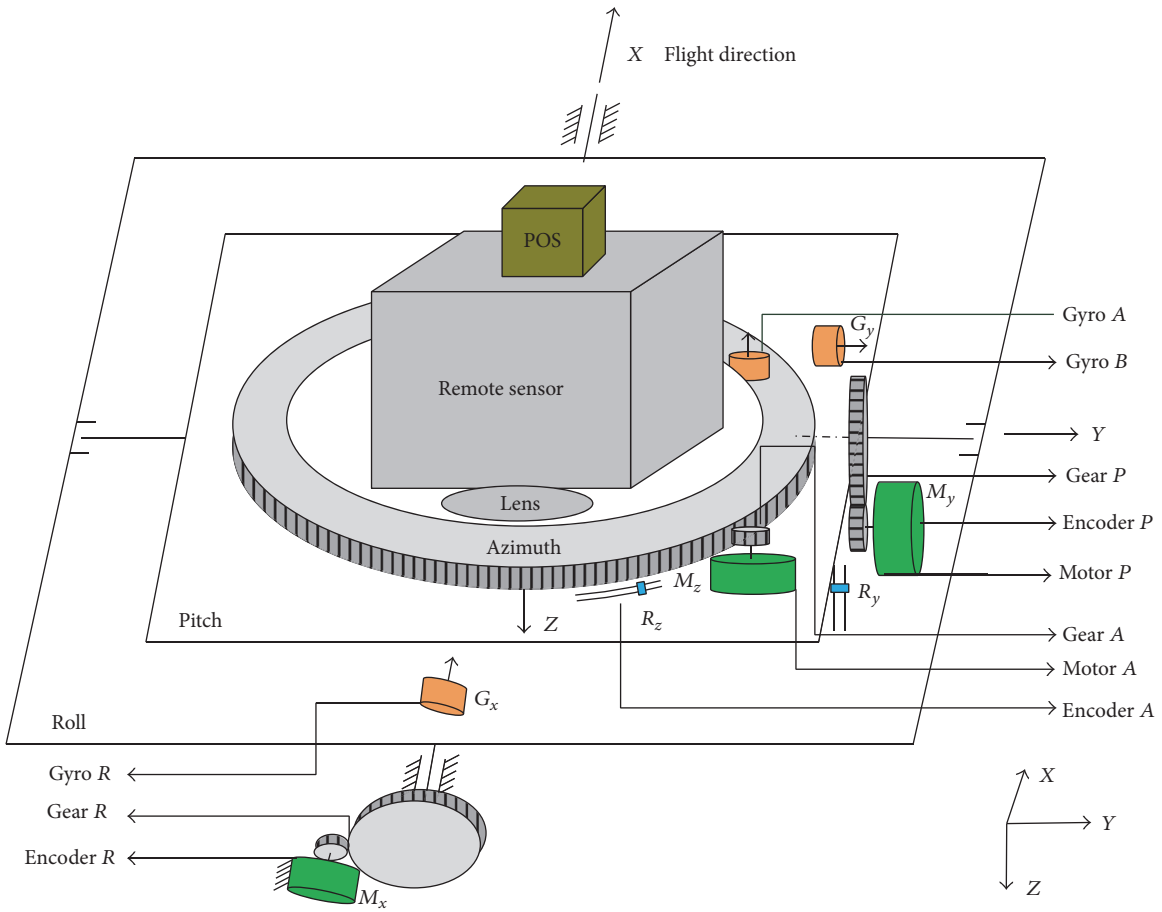

Figure 2: Schematic diagram of the three-axis ISP's working principle.

in inertial space for control system of ISP and imaging sensor through measuring the angular movement of imaging sensor.

2.2. Working Principal of ISP. Figure 2 shows the schematic diagram of the three-axis ISP principle. We can see that the ISP consists of three gimbals, which are azimuth gimbal (A-gimbal), pitch gimbal (P-gimbal), and roll gimbals (R-gimbal). Among them, the A-gimbal is assembled on the P-gimbal and can rotate around Z_a axis. Likewise, the P-gimbal is assembled on the R-gimbal and can rotate around X_p axis. The R-gimbal is assembled on the base of aviation platform and can rotate around Y_r axis. From Figure 2, we can see the relationships between three gimbals: G_p, G_r, and G_a, respectively, stand for rate gyro that measures inertial angular rate of P-gimbals, R-gimbals, and A-gimbals. E_x, E_p, and E_a, respectively, stand for photoelectric encoder which measures relative angular between gimbals. M_r, M_p, and M_a, respectively, stand for gimbals servo motor which drives R-gimbals, P-gimbal, and A-gimbal to keep these three gimbals steady in inertial space. Ax and Ay, respectively, represent accelerometers installed on the R-gimbal and R-gimbal used to measure the gimbals' rotary angular acceleration. E_x and E_y represent encoders installed on two leveling gimbals to detect the gimbals' rotary angular position.

2.3. Three-Closed Loop Compound Control Scheme. Conventional stabilization techniques employ rate gyros, rate integrating gyros, or rate sensors to sense rate disturbances about the LOS. Figure 3 shows the block diagram of traditional three-loop control system for ISP. In Figure 3, the blocks of G-pos, G-spe, and G-cur separately represent the controllers in the position loop, speed loop, and current loop; the PWM block represents the power amplification used for the current amplification to drive the torque motor; L represents the inductance of a torque motor and R represents the resistance; K_t represents the torque coefficient of the motor and N is the transition ratio from the torque motor to the gimbals; J_m represents the moment of inertia of the motor and J_l represents the moment of inertia of the gimbals along the rotation axis.

Figure 4 shows the process model of the ISP control scheme block diagram. G_{AP}, G_{PP}, and G_{RP} are the PID controllers for position loop of azimuth gimbal, pitch gimbal, and roll gimbal, respectively. G_{AR}, G_{PR}, and G_{RR} are the PID controllers for rate loop of azimuth gimbal, pitch gimbal,

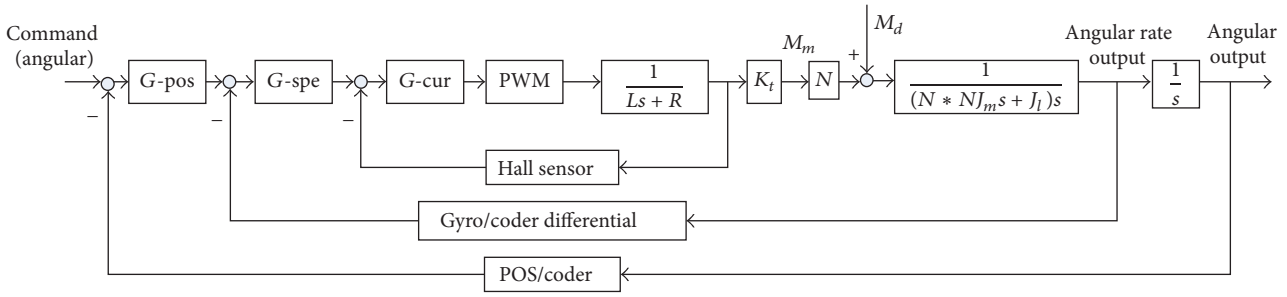

Figure 3: A block diagram of traditional three-loop control system for ISP.

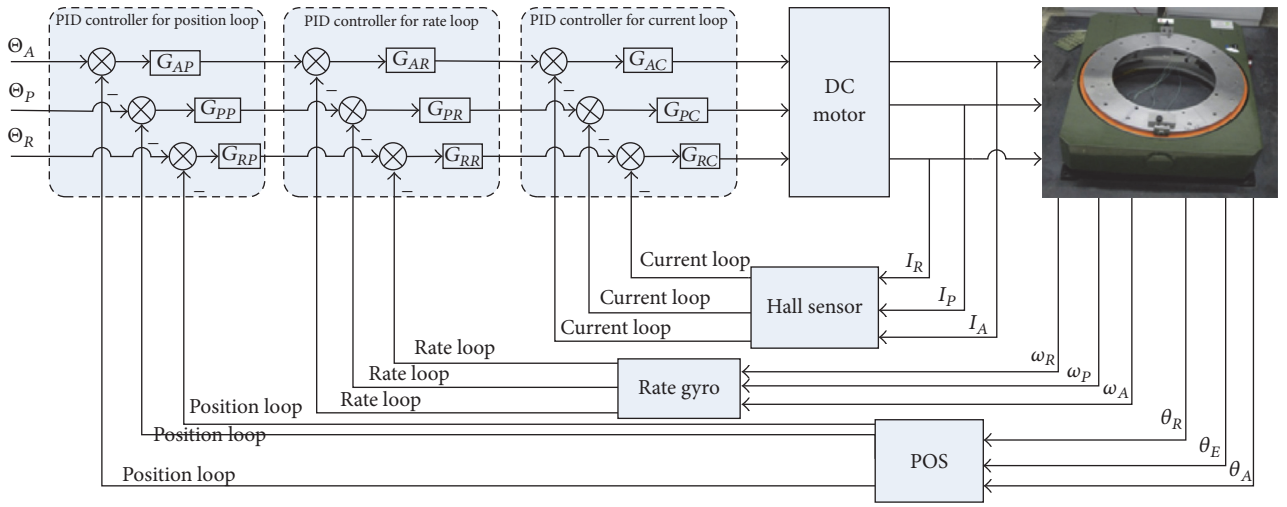

Figure 4: The process model of the ISP control scheme block diagram.

and roll gimbal, respectively. G_{AC}, G_{PC}, and G_{RC} are the PID controllers for current loop of azimuth gimbal, pitch gimbal, and roll gimbal, respectively.

3. Dynamic Modeling of the Mass Unbalance Torque

Due to the influence of mechanical structure design and machining accuracy, three-axe ISP's center of mass is not coincident with the center of rotating shaft completely. So, when there is acceleration that acted on the ISP gimbals, the mass unbalance torque disturbance occurs [23], which will severely degrade the system control accuracy. Mass unbalance torque under the static base is caused by both of the gravity and gimbal acceleration.

The mass imbalance produces LOS jitter when the payload center of gravity is not centered on an axis of rotation for the gimbals. Linear vibration, acting through the lever arm of the center of gravity offset, thus produces torque disturbances. When an ISP is working at a flying aircraft, due to both effects of gravity acceleration and the motion acceleration of ISP's gimbals and imaging sensors, the mass imbalance torque occurs. Figure 5 shows the schematic diagram of the functional mechanism of mass imbalance torque under moving base and static base, respectively.

In Figure 5(a), l_x and l_z, respectively, stand for the eccentric lever arms of mass center of ISP relative to a horizontal rotation axis (x or y) and the vertical axis-z. a_f and a_z, respectively, stand for the horizontal and vertical interference accelerated speed during movement acting on the gimbal and g stands for acceleration of gravity. If we take the counterclockwise direction as a positive direction, imbalance torque can be expressed as

$$T_{\text{im}} = -m\left(a_z + g\right) \cdot l_x - m \cdot a_f \cdot l_z, \tag{1}$$

where T_{im} is the unbalance torque of the moving base and m is the total mass of the frame and the load,

$$T_{\text{motor}} = -\frac{T_{\text{im}}}{N} = -\frac{1}{N}\left[-m\left(a_z + g\right) \cdot l_x - m \cdot a_f \cdot l_z\right], \tag{2}$$

where T_{motor} is the extra unbalance torque produced by motor. N is the transmission ratio.

The unbalance torque caused by gravity can be expressed as

$$T_g = mgl_z \sin\theta - mgl_x \cos\theta. \tag{3}$$

Since the leveling angles of ISP are changed in a small range of about $\theta = \pm 5^{\circ}$, the cosine and sine function values of θ are approximately equal to 1 and 0, respectively, so the

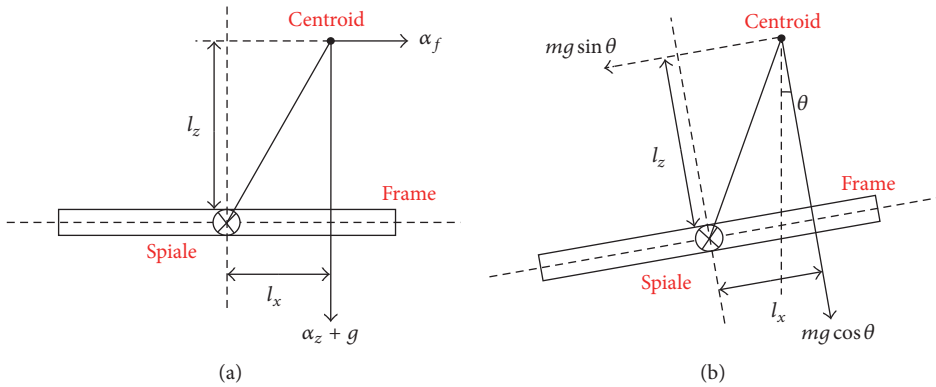

FIGURE 5: The geometrically schematic diagram to show the functional mechanism of mass imbalance torque: (a) under moving base condition and (b) under static base condition.

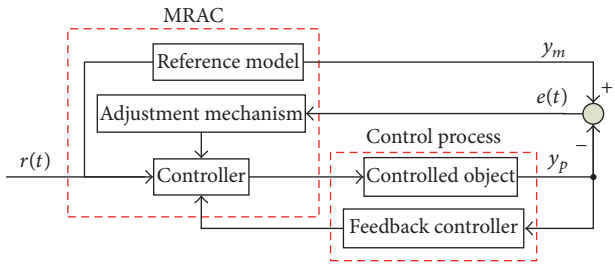

FIGURE 6: The structure of a model reference adaptive control (MRAC) system.

unbalance torque caused by gravity can be further expressed as

$$T_g = -mgl_x \cos\theta. \tag{4}$$

4. MRAC/PID Compound Controller Design

4.1. Adaptive Model Reference Control Principal. Figure 6 shows the structure of an adaptive model reference control (MRAC) system. It is composed of four components, that is, control process, controller, reference model, and adjustment mechanism block [30].

The adaptive model reference control (MRAC) technique is used for devising a controller based on the information y_m, y_p, $r(t)$, and $e(t)$. The adaptive mechanism automatically adjusts controller parameters so that the behavior of the closed loop control plant output y_p closely follows that of y_m of the reference model. Parameters and structure of reference model are specified on the base of requirements of control performance. The adjustment mechanism of MRAC system is constructed by adaptive control rule, which performs the algorithms as follows.

Tracking error is defined as

$$e = y_m - y_p, \tag{5}$$

where e is error of input and output, y_m is the output of the reference model, and y_p is the output of the actual system. Thus, e will eventually be close to a constant or 0. If e is bounded, then y_p is bounded. So the control system is convergent under this controller.

4.2. MRAC/PID Compound Controller. PID control is one of the most commonly used control methods in engineering. It has the advantages of simple algorithm and high reliability, but it needs more accurate system model [31]. When the input signal is applied to a variable structure control system, the system should be stable while altering controller coefficients according to control error signal.

According to Figure 3, the bandwidth of the current loop is much larger than the bandwidth of the stable loop, so the current loop is regarded as a proportional component with coefficient of 1. The transfer functions of the G-pos and G-spe are too small and can be equivalent to 1. $k_c((\tau_c s + 1)/s)$ is the transfer function of G-cur, and $U/(T_{\mathrm{PWM}}S + 1)$ is the transfer function of the PWM [32]. In the simulation, the values of these parameters are too small to be ignored for 0, such as L, N, τ_c, T_{PWM}, and J_m. So the ISP control system is established as the two-order system model.

Based on [29, 30], the controller is designed as follows:

$$J(\theta) = \frac{1}{2}e^2(\theta), \tag{6}$$

where the time rate of change of θ stands for proportional to negative gradient of J,

$$\frac{d\theta}{dt} = -\gamma\frac{\partial J}{\partial \theta} = -\gamma e\frac{\partial e}{\partial \theta}, \tag{7}$$

where θ stands for the controller parameter vector. The components of $\partial e/\partial\theta$ stand for the sensitivity derivatives of the error with respect to θ. The parameter γ stands for known as the adaptation gain.

Considering an aerial ISP system described by second-order model $b/(s^2+\alpha_1 s+\alpha_2)$, the closed loop transfer function is

$$\frac{y_p(s)}{r(s)} = \frac{b\left(K_d s^2 + K_p s + K_i\right)}{s\left(s^2 + \alpha_1 s + \alpha_2\right) + b\left(K_d s^2 + K_p s + K_i\right)}, \quad (8)$$

$$\frac{y_p(s)}{r(s)} = \frac{b\left(K_d s^2 + K_p s + K_i\right)}{s^3 + \left(\alpha_1 + bK_d\right)s^2 + \left(\alpha_2 + bK_p\right)s + bK_i}. \quad (9)$$

From (9) and required performance of system, we obtain a reference model as follows:

$$\frac{y_m(s)}{r_m(s)} = \frac{b_{m1}s^2 + b_{m2}s + b_{m3}}{s^3 + a_{m1}s^2 + a_{m2}s + a_{m3}}, \quad (10)$$

where $a_{m1} = \alpha_1 + bK_d$, $a_{m2} = \alpha_2 + bK_p$, $a_{m3} = bK_i$, $b_{m1} = bK_d$, $b_{m2} = bK_p$, and $b_{m3} = bK_i$.

The values of PID controller parameters are determined, K_p, K_i, and K_d, in

$$\begin{aligned}
\frac{dK_p}{dt} &= -\gamma_p \frac{\partial J}{\partial K_p} = -\gamma_p \left(\frac{\partial J}{\partial e}\right)\left(\frac{\partial e}{\partial y_p}\right)\left(\frac{\partial y_p}{\partial K_p}\right),\\
\frac{dK_i}{dt} &= -\gamma_i \frac{\partial J}{\partial K_i} = -\gamma_i \left(\frac{\partial J}{\partial e}\right)\left(\frac{\partial e}{\partial y_p}\right)\left(\frac{\partial y_p}{\partial K_i}\right),\\
\frac{dK_d}{dt} &= -\gamma_d \frac{\partial J}{\partial K_d} = -\gamma_d \left(\frac{\partial J}{\partial e}\right)\left(\frac{\partial e}{\partial y_p}\right)\left(\frac{\partial y_p}{\partial K_d}\right),
\end{aligned} \quad (11)$$

where $\partial J/\partial e = e$, $\partial e/\partial y = 1$, $D = d/dt$, and

$$\begin{aligned}
\frac{\partial y_p}{\partial K_p} &= \frac{bD}{D^3 + \left(\alpha_1 + bK_d\right)D^2 + \left(\alpha_2 + bK_p\right)D + bK_i} \cdot \left[r - y_p\right],\\
\frac{\partial y_p}{\partial K_i} &= \frac{b}{D^3 + \left(\alpha_1 + bK_d\right)D^2 + \left(\alpha_2 + bK_p\right)D + bK_i} \cdot \left[r - y_p\right],\\
\frac{\partial y_p}{\partial K_d} &= \frac{bD^2}{D^3 + \left(\alpha_1 + bK_d\right)D^2 + \left(\alpha_2 + bK_p\right)D + bK_i} \cdot \left[r - y_p\right].
\end{aligned} \quad (12)$$

Then dK_p/dt, dK_i/dt, and dK_d/dt can be derived by

$$\begin{aligned}
\frac{dK_p}{dt} &= -\gamma_p \frac{\partial J}{\partial K_p}\\
&= -\gamma_p e \frac{bD}{D^3 + \left(a_1 + bK_d\right)D^2 + \left(a_2 + bK_p\right)D + bK_i} \cdot \left[r - y_p\right],\\
\frac{dK_i}{dt} &= -\gamma_i \frac{\partial J}{\partial K_i}\\
&= -\gamma_i e \frac{b}{D^3 + \left(a_1 + bK_d\right)D^2 + \left(a_2 + bK_p\right)D + bK_i} \cdot \left[r - y_p\right],\\
\frac{dK_d}{dt} &= -\gamma_d \frac{\partial J}{\partial K_d}\\
&= -\gamma_d e \frac{bD^2}{D^3 + \left(a_1 + bK_d\right)D^2 + \left(a_2 + bK_p\right)D + bK_i} \cdot \left[r - y_p\right].
\end{aligned} \quad (13)$$

If the adaptive control law is given, the system can guarantee the stability of the system under the action of the model reference adaptive PID controller and can achieve the control goal. Thus, a new PID control based on the reference model is formed. The basic structure of the MRAC/PID compound control system is shown in Figure 7. In Figure 7, the blocks of G-pos, G-spe, and G-cur separately represent the controllers; the PWM block represents the power amplification used for the current amplification to drive the torque motor.

5. Simulation Analysis

5.1. Tracking Performance. According to the adaptive model reference control (MRAC) method, through the parameters adjustment simulation environment, the system can get the ideal output.

The PID parameter values of the reference model are selected by the parameter tuning or the test calculation method, as shown in Figures 8 and 9.

So the result of the PID parameter value is selected and taken out by the reference of the automatic adjustment: $K_p = 10$, $K_i = 0$, and $K_d = 4$. Based on the fixed parameters in the three-loop control system of ISP, the reference model is

$$\frac{y_m(s)}{r_m(s)} = \frac{55.44 + 221.76s + 7.56s^2}{55.44 + 221.76s + 7.56s^2 + 0.018s^3}. \quad (14)$$

Further, by (14), the control strategy of the adaptive PID controller is adjusted by the MRAC/PID compound controller, and the stability and accuracy of the system are improved continuously.

First, the responses for the step input are analyzed. Figure 10 shows the system response curve and its partial

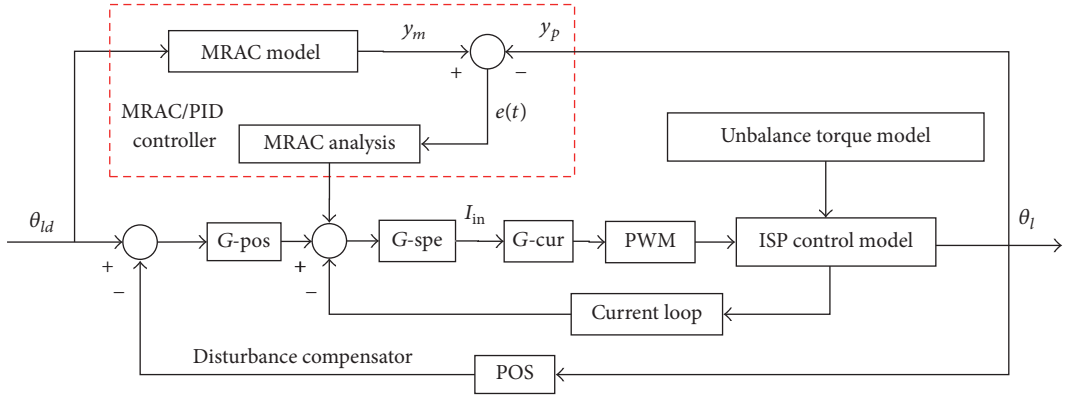

Figure 7: Block diagram of MRAC/PID compound controller.

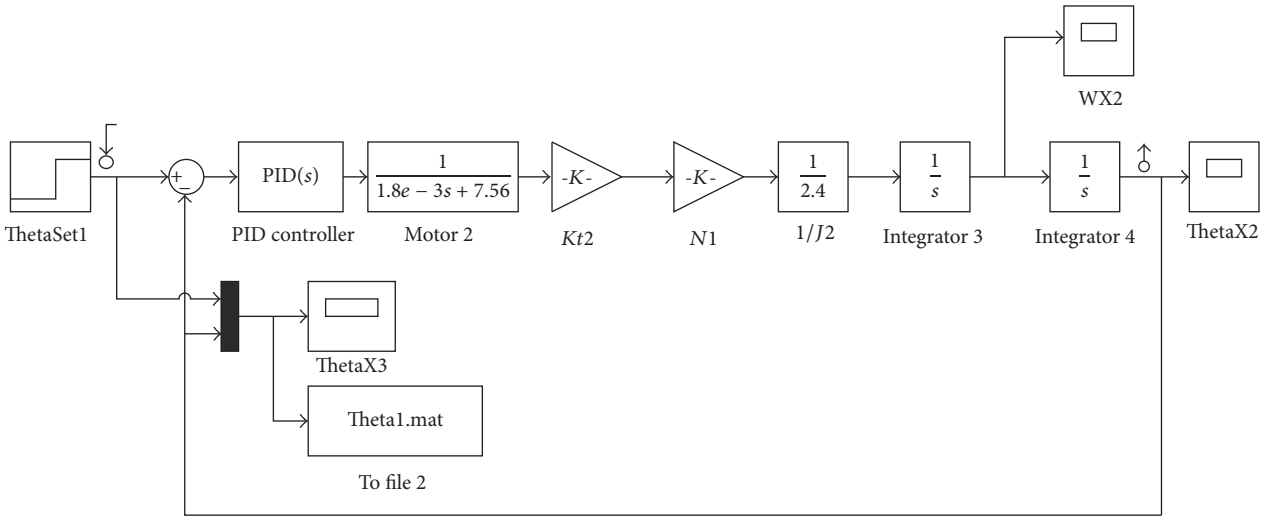

Figure 8: Automatic adjustment of PID parameters for reference model design.

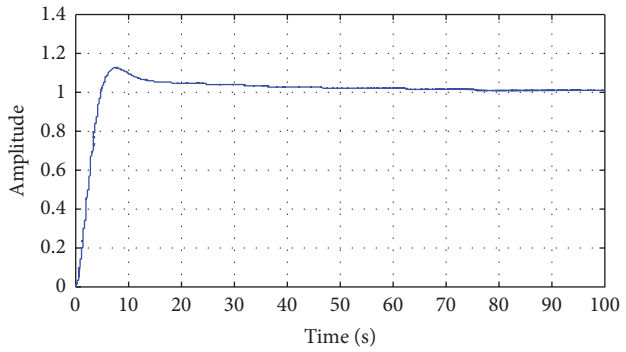

Figure 9: Automatic adjustment of PID parameters model.

enlarged detail for the traditional PID controller and the MRAC/PID compound controller. As seen in the figures, compared with PID control, the stability time and accuracy of the MRAC/PID compound control are much shorter and higher.

5.2. Adaptive PID Parameters. Figure 11 shows the parameters variation curves of the MRAC/PID compound controller.

From Figures 10 and 11, we see that the MRAC/PID compound control scheme can obviously improve the accuracy of the control system. Under the same unbalance torque disturbance conditions, the position output peak-valley errors of MRAC/PID compound scheme and traditional PID control method are +0.0075° to −0.006° and +0.035° to −0.05°, respectively, meaning that the position accuracy is improved up to 84.1% after MRAC/PID scheme applied. The simulation results illustrate the compound scheme has high disturbance rejection ability compared with the PID controller.

6. Experimental Verification

In order to validate the proposed MRAC/PID compound scheme, the experiments are then performed, which are conducted on a three-axis ISP.

According to the specific functional requirements of the system, the system hardware circuit is designed. Figure 12

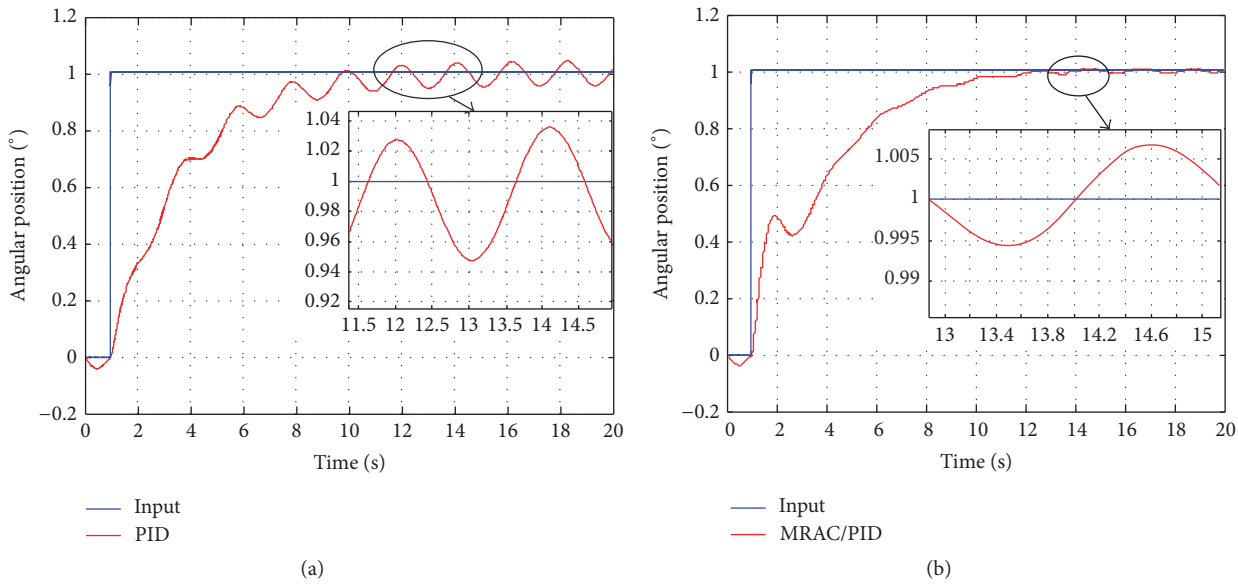

FIGURE 10: System response curves and partial enlarged detail for the (a) traditional PID controller and (b) MRAC/PID compound controller.

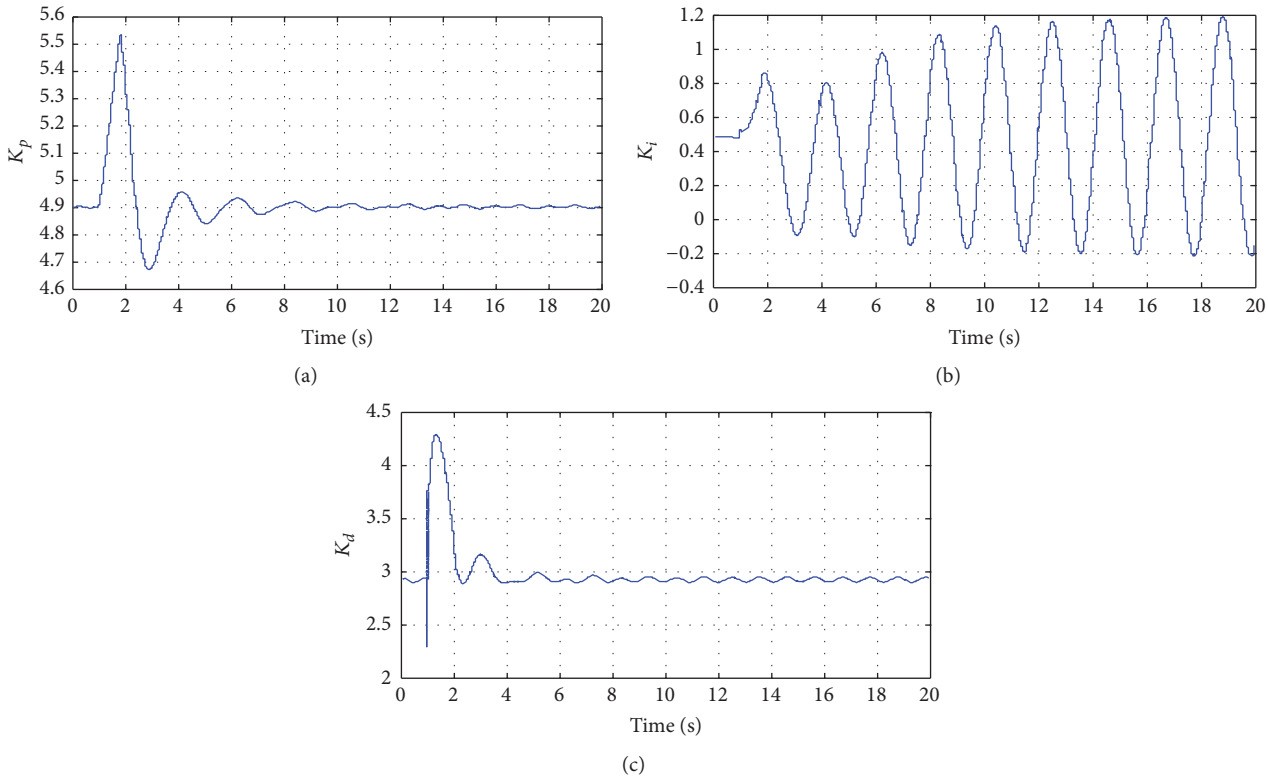

FIGURE 11: The parameter variation curves of the MRAC/PID compound controller: (a) K_p parameter; (b) K_i parameter; (c) K_d parameter.

shows the hardware control system circuit connection diagram of three-axis ISP. The main functional devices are DC torque motor, POS, gyroscope, encoder, and so forth.

The main program flowchart is shown in Figure 13. After the system is reset and the external device is initialized, the external device interrupt is opened. The six interrupt management procedures include ADC sequencer ADCSEQ interrupt, interrupt timer CPU-Timer 0, SPI receiving interrupt, SCI A sending/receiving interrupt, SCI B sending/receiving interrupt, and SCI C receiving interrupt using the software

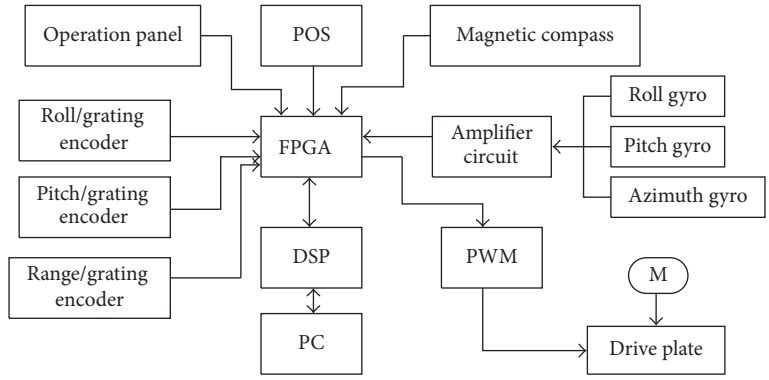

Figure 12: Hardware control system circuit connection diagram.

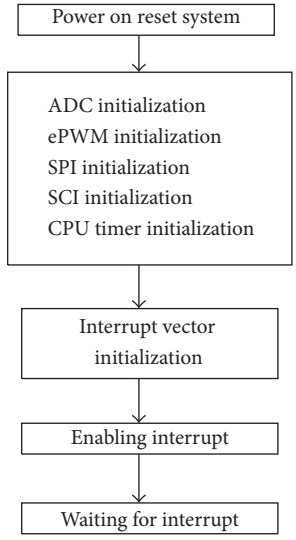

Figure 13: Main program flowchart.

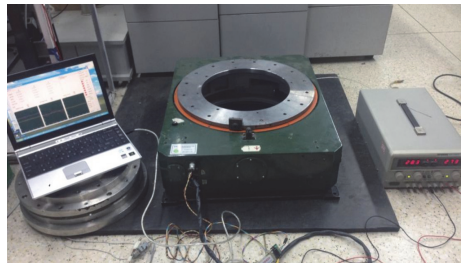

Figure 14: The three-axis ISP experimental system.

system of the platform. Platform interrupt priority order is ADCSEQ > CPU-Timer 0 > SPI > SCI A > SCI B > SCI C.

Figure 14 shows the picture of the experimental system. The main parameters of the ISP are as follows: maximum load and self-weight are, respectively, 80 kg and 40 kg, the maximum leveling rotation angle range is ±5°, and the maximum heading rotation angle range is ±25°. In the experiments, the artificial load is 20 kg and the power supply voltage is 28 V. As

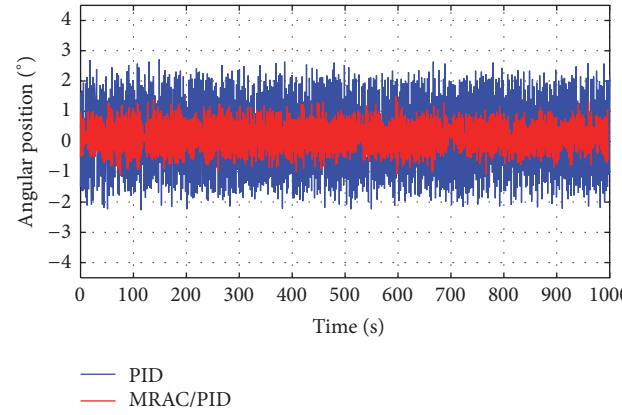

Figure 15: Experiment comparison between the PID and adaptive MRAC/PID controllers under unbalance disturbance.

a comparison, the results obtained by PID controller are also displayed.

The experiments are designed aiming at rejecting unbalanced torque disturbance. From (4), we know that the unbalance torque is nonlinear and time-varying with characteristic of cosine function. Therefore, the cosine interference component is artificially added into the current loop of the gimbal system to represent the unbalance torque disturbance. Thus, we can evaluate the disturbance rejection ability of the compound scheme.

Figure 15 shows the experiment comparison between the PID and adaptive MRAC/PID controllers when the interference current $I = 0.5\cos(0.4\pi t) + \cos(0.9\pi t)$. We can see that, for the MRAC/PID and PID controllers, the output error ranges of the attitude angle are about ±1° and ±2°, respectively. Obviously, compared with the PID controller, the position accuracy is improved up to nearly 50% by the MRAC/PID compound controller.

7. Conclusion

In this paper, to suppress the nonlinear and time-varying mass unbalance torque disturbance of the aerial-axis inertially stabilized platform (ISP), a compound control scheme

based on both of model reference adaptive control (MRAC) and PID control methods is proposed. In this way, the tracking accuracy and stability of the ISP are improved significantly. To verify the method, the simulations and experiments are, respectively, carried out. The results show that MRAC/PID compound scheme is good at the disturbance rejection. Compared with the PID, the tracking accuracy of the MRAC/PID compound controller is improved by about 50%.

Competing Interests

The authors declare that there is no conflict of interests regarding the publication of this paper.

Acknowledgments

This work was funded by the National Natural Science Foundation of China (nos. 51375036, 51205019, and 61573040) and the China Scholarship Council (CSC).

References

[1] X. Zhou, H. Zhang, and R. Yu, "Decoupling control for two-axis inertially stabilized platform based on an inverse system and internal model control," *Mechatronics*, vol. 24, no. 8, pp. 1203–1213, 2014.

[2] M. K. Masten, "Inertially stabilized platforms for optical imaging systems," *IEEE Control Systems Magazine*, vol. 28, no. 1, pp. 47–64, 2008.

[3] J. M. Hilkert, "Inertially stabilized platform technology: concepts and principles," *IEEE Control Systems Magazine*, vol. 28, no. 1, pp. 26–46, 2008.

[4] P. J. Kennedy and R. L. Kennedy, "Direct versus indirect line of sight (LOS) stabilization," *IEEE Transactions on Control Systems Technology*, vol. 11, no. 1, pp. 3–15, 2003.

[5] X. Zhou, Y. Jia, Q. Zhao, and T. Cai, "Dual-rate-loop control based on disturbance observer of angular acceleration for a three-axis aerial inertially stabilized platform," *ISA Transactions*, vol. 63, pp. 288–298, 2016.

[6] M. M. Abdo, A. R. Vali, A. R. Toloei, and M. R. Arvan, "Stabilization loop of a two axes gimbal system using self-tuning PID type fuzzy controller," *ISA Transactions*, vol. 53, no. 2, pp. 591–602, 2014.

[7] J. L. Miller, S. Way, B. Ellison, and C. Archer, "Design challenges regarding high-definition electro-optic/infrared stabilized imaging systems," *Optical Engineering*, vol. 52, no. 6, Article ID 061310, 2013.

[8] W. W. Zhang, *System Identification and Modeling on the Combustion System of Industry Boiler*, Shanghai Jiao Tong University, Shanghai, China, 2007.

[9] J. G. Fu, *Design and Research of Inertial Platform Stabilization Loop*, Harbin Engineering University, Harbin, China, 2005.

[10] X. Song, H. Chen, and Y. Xue, "Stabilization precision control methods of photoelectric aim-stabilized system," *Optics Communications*, vol. 351, Article ID 20107, pp. 115–120, 2015.

[11] B. Yang and J. Wang, "Hybrid control based on improved CMAC for motor-driven loading system," *Hangkong Xuebao/Acta Aeronautica et Astronautica Sinica*, vol. 29, no. 5, pp. 1314–1318, 2008.

[12] W. Ji, Q. Li, and B. Xu, "Design study of adaptive fuzzy PID controller for LOS stabilized system," in *Proceedings of the 6th International Conference on Intelligent Systems Design and Applications (ISDA '06)*, pp. 336–341, Washington, DC, USA, October 2006.

[13] Y. Han, Y. Lu, and H. Qiu, "An improved control scheme of gyro stabilization electro-optical platform," in *Proceedings of the IEEE International Conference on Control and Automation (ICCA '07)*, pp. 346–351, Guangzhou, China, June 2007.

[14] J. X. Zhao, G. Su, and L. Y. Hao, "Modeling and simulation of strapdown stabilization platform," *Fire and Command Control*, vol. 33, no. 4, pp. 101–106, 2008.

[15] G. Abitova, M. Beisenbi, and V. Nikulin, "Design of a control system with high robust stability characteristics," in *Proceedings of the IEEE 3rd International Congress on Ultra Modern Telecommunications and Control Systems and Workshops (ICUMT '11)*, pp. 1–5, Budapest, Hungary, 2011.

[16] Z. Y. Tang, Z. C. Pei, and B. L. Wu, "Research on image-stabilizing system based on gyro-stabilized platform with reflector," in *Proceedings of the 7th International Symposium on Instrumentation and Control Technology: Measurement Theory and Systems and Aeronautical Equipment*, pp. 1156–1168, October 2008.

[17] G. N. Zhang, Z. G. Liu, S. L. Yao, Y. C. Liao, and C. Xiang, "Suppression of low-frequency oscillation in traction network of high-speed railway based on auto-disturbance rejection control," *IEEE Transactions on Transportation Electrification*, vol. 2, no. 2, pp. 244–255, 2016.

[18] X. Zhou, Y. Jia, Q. Zhao, and R. Yu, "Experimental validation of a compound control scheme for a two-axis inertially stabilized platform with multi-sensors in an unmanned helicopter-based airborne power line inspection system," *Sensors*, vol. 16, no. 3, pp. 366–381, 2016.

[19] M.-C. Zhu, H. Liu, X. Zhang, and H.-G. Jia, "Adaptive feedforward control for inertially stabilized platform," *Optics and Precision Engineering*, vol. 23, no. 1, pp. 141–148, 2015.

[20] Y. Wang, X. Lu, and S. Wang, "Double close loop electrode regulator system based on active disturbance rejection control technology," in *Proceedings of the 2nd International Symposium on Information Science and Engineering (ISISE '09)*, pp. 565–569, December 2009.

[21] L. Wang, *Research on Tension Control System Based on Model Reference Adaptive Algorithm*, Central South University, Changsha, China, 2008.

[22] J. M. Hilkert and D. A. Hullender, "Adaptive control system techniques applied to inertial stabilization systems," in *Acquisition, Tracking, and Pointing IV*, vol. 1304 of *Proceedings of SPIE*, pp. 190–206, International Society for Optical Engineering, Orlando, Fla, USA, September 1990.

[23] C.-L. Lin and Y.-H. Hsiao, "Adaptive feedforward control for disturbance torque rejection in seeker stabilizing loop," *IEEE Transactions on Control Systems Technology*, vol. 9, no. 1, pp. 108–121, 2001.

[24] A. G. Rodriâguez, R. M. Herrera, V. F. Batlle, and P. P. Sanjuan, "Improving the mechanical design of new staircase wheelchair," *Industrial Robot*, vol. 34, no. 2, pp. 110–115, 2007.

[25] S.-K. Oh, W.-D. Kim, W. Pedrycz, and B.-J. Park, "Polynomial-based radial basis function neural networks (P-RBF NNs) realized with the aid of particle swarm optimization," *Fuzzy Sets and Systems*, vol. 163, no. 1, pp. 54–77, 2011.

[26] R.-E. Precup, M.-B. Rădac, M. L. Tomescu, E. M. Petriu, and S. Preitl, "Stable and convergent iterative feedback tuning of fuzzy

controllers for discrete-time SISO systems," *Expert Systems with Applications*, vol. 40, no. 1, pp. 188–199, 2013.

[27] X. Lei, S. S. Ge, and J. Fang, "Adaptive neural network control of small unmanned aerial rotorcraft," *Journal of Intelligent & Robotic Systems: Theory and Applications*, vol. 75, no. 2, pp. 331–341, 2014.

[28] M. Sawada and K. Itamiya, "A design scheme of model reference adaptive control system with using a smooth parameter projection adaptive law," in *Proceedings of the SICE Annual Conference (SICE '11)*, pp. 1704–1709, Tokyo, Japan, September 2011.

[29] S. L. Xiao, Y. M. Li, and J. G. Liu, "A model reference adaptive PID control for electromagnetic actuated micro-positioning stage," in *Proceedings of the IEEE International Conference on Automation Science and Engineering (CASE '12)*, pp. 97–102, Seoul, South Korea, August 2012.

[30] P. Kungwalrut, M. Thumma, V. Tipsuwanporn, A. Numsomran, and P. Boonsrimuang, "Design MRAC PID control for fan and plate process," in *Proceedings of the 50th Annual Conference on Society of Instrument and Control Engineers (SICE '11)*, pp. 2944–2948, September 2011.

[31] H. Ouyang, J. Yue, and Y. Su, "Design and application of PID controllers based on interval computing theory," in *Proceedings of the 2nd Annual Conference on Electrical and Control Engineering (ICECE '11)*, pp. 1505–1510, Yichang, China, September 2011.

[32] J.-C. Fang, Z.-H. Qi, and M.-Y. Zhong, "Feedforward compensation method for three axes inertially stabilized platform imbalance torque," *Journal of Chinese Inertial Technology*, vol. 18, no. 1, pp. 38–43, 2010.